Article

Current Biology

Scaling, Selection, and Evolutionary Dynamics of the Mitotic Spindle

Highlights

- Spindles exhibit extensive variations between individuals of the same species
- Variations in spindles are correlated with variations in cell size
- In nematodes, embryo size, and thus cell size, is subject to stabilizing selection
- Selection on cell size explains within- and between-species variations in spindles

Authors

Reza Farhadifar, Charles F. Baer, ..., Marie Delattre, Daniel J. Needleman

Correspondence

rfarhadifar@cgr.harvard.edu

In Brief

Farhadifar et al. show that the mitotic spindle exhibits extensive variation both within and between closely related species. The effect of mutation on the spindle, together with stabilizing selection on embryo size, quantitatively explains the levels of within-species variation in the spindle and its diversity over 100 million years of evolution.

Farhadifar et al., 2015, Current Biology *25*, 1–9
March 16, 2015
http://dx.doi.org/10.1016/j.cub.2014.12.060

CellPress

Please cite this article in press as: Farhadifar et al., Scaling, Selection, and Evolutionary Dynamics of the Mitotic Spindle, Current Biology (2015), http://dx.doi.org/10.1016/j.cub.2014.12.060

Current Biology 25, 1–9, March 16, 2015 ©2015 Elsevier Ltd All rights reserved http://dx.doi.org/10.1016/j.cub.2014.12.060

Article

Scaling, Selection, and Evolutionary Dynamics of the Mitotic Spindle

Reza Farhadifar,[1,*] Charles F. Baer,[2] Aurore-Cécile Valfort,[3] Erik C. Andersen,[4] Thomas Müller-Reichert,[5] Marie Delattre,[3] and Daniel J. Needleman[1]

[1]School of Engineering and Applied Sciences, Department of Molecular and Cellular Biology, FAS Center for Systems Biology, Harvard University, Cambridge, MA 02138, USA

[2]Department of Biology and University of Florida Genetics Institute, University of Florida, Gainesville, FL 32611, USA

[3]Laboratory of Molecular Biology of the Cell, UMR 5239, Ecole Normale Supérieure de Lyon, Centre National de la Recherche Scientifique, 69007 Lyon, France

[4]Department of Molecular Biosciences, Northwestern University, Evanston, IL 60208, USA

[5]Experimental Center, Faculty of Medicine Carl Gustav Carus, Technische Universität Dresden, Fiedlerstrasse 42, 01307 Dresden, Germany

Summary

Background: Cellular structures such as the nucleus, Golgi, centrioles, and spindle show remarkable diversity between species, but the mechanisms that produce these variations in cell biology are not known.

Results: Here we investigate the mechanisms that contribute to variations in morphology and dynamics of the mitotic spindle, which orchestrates chromosome segregation in all Eukaryotes and positions the division plane in many organisms. We use high-throughput imaging of the first division in nematodes to demonstrate that the measured effects of spontaneous mutations, combined with stabilizing selection on cell size, are sufficient to quantitatively explain both the levels of within-species variation in the spindle and its diversity over ~100 million years of evolution. Furthermore, our finding of extensive within-species variation for the spindle demonstrates that there is not just one "wild-type" form, rather that cellular structures can exhibit a surprisingly broad diversity of naturally occurring behaviors.

Conclusions: Our results argue that natural selection acts predominantly on cell size and indirectly influences the spindle through the scaling of the spindle with cell size. Previous studies have shown that the spindle also scales with cell size during early development. Thus, the scaling of the spindle with cell size controls its variation over both ontogeny and phylogeny.

Introduction

Cellular structures such as the nucleus [1], Golgi [2], centrioles [3], and spindle [4–6] show remarkable diversity between species. The mechanisms that produce these variations in cell biology are not known, and a wide variety of possibilities have been proposed. Some have hypothesized that nearly all subcellular processes have been molded by natural selection to perform optimally in their native cellular and environmental context [7]. Others have suggested that natural selection has only had a limited role in shaping subcellular organization, with variation arising either from an accumulation of non-adaptive changes [8, 9] or due to the intrinsic tendency of self-organizing, living matter [10]. Different processes could dominate in different systems and on different evolutionary timescales [11]. Each of these, and other possibilities, makes distinct assertions of how spontaneous mutations modify cell biological processes, of the fitness effects of these changes, and of the trends in these changes over the course of evolution. For example, neutral traits are broadly distributed in populations with a mean value that diverges as the square root of the number of generations to their last common ancestor, whereas optimized traits change over evolution due to changes in the optimum (not due to phylogenetic distances per se) and are degraded by spontaneous mutations [12]. The spindle, which segregates chromosomes during cell division in all Eukaryotes, is one of the most extensively studied subcellular structures, but even in this case the validity of different evolutionary scenarios cannot currently be tested because there are insufficient data on the influence of spontaneous mutations on spindles, the relationship between spindles and fitness, and evolutionary trends in spindles.

Evolutionary trends can be studied in extant organisms by either investigating changes across species of known phylogeny [13] or by dissecting the nature and extent of within-species variations [14]. There is extensive information in different species on the morphology and dynamics of the spindle [4, 5, 15, 16]. This work has revealed large variations in all attributes of the spindle, with the length of the spindle ranging from ~0.5 μm in *Ostreococcus tauri* [17] to over 50 μm in early development in *Xenopus laevis* [18], but most of the data are from distantly related organisms of unknown phylogenetic relationship, making it difficult to determine evolutionary trends. The most detailed comparison between spindles in more closely related species has been between *X. laevis* and *X. tropicalis* [19–21], which are still quite distant, having diverged ~40 million years ago; they have undergone extensive genetic changes including a whole-genome duplication [22, 23]. We are unaware of any study of the extent of within-species variations in spindle morphology or dynamics. Thus, the evolutionary trends in changes in the spindle remain unknown.

The ultimate source of biological diversity is mutations, which are subjected to selection, drift, and recombination, to produce variation within species and, over longer timescales, differences between species. The manner in which genetic changes caused by spontaneous mutations alter the spindle is thus critical for determining its evolution. Studies in different model organisms have identified hundreds of proteins that contribute to the spindle [15, 16], but this information cannot easily be used to infer the effects of spontaneous mutations on the spindle, which depends on the detailed spectrum of rates and location of mutation in the genome that occur in both protein coding and regulator regions. Analysis of DNA sequences provides insight into the conservation and variations in proteins known to contribute to the spindle in model organisms, for example revealing that no mitotic molecular motor is universally conserved [24, 25], but it is unclear how to relate these data to changes in spindle morphology and dynamics. Thus, the manner in which spontaneous mutations cause

*Correspondence: rfarhadifar@cgr.harvard.edu

Please cite this article in press as: Farhadifar et al., Scaling, Selection, and Evolutionary Dynamics of the Mitotic Spindle, Current Biology (2015), http://dx.doi.org/10.1016/j.cub.2014.12.060

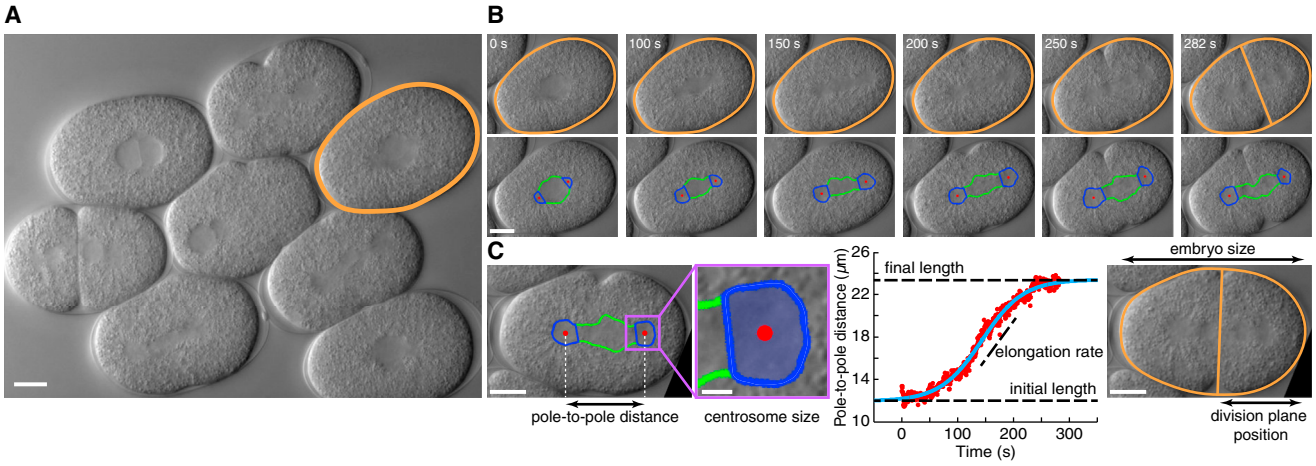

Figure 1. Tracking and Quantification of Spindle Traits in the First Mitotic Division of *C. elegans*

(A) Live-cell imaging of multiple embryos. The embryo in (B) is highlighted. The scale bar represents 10 μm.

(B) Automatic tracking of the cellular boundary (orange), centrosomes (blue), and spindle region (green). The division plane is marked in the last top panel. The scale bar represents 10 μm.

(C) Quantification of cell-division traits. For each embryo, we measured the pole-to-pole distance of the spindle as a function of time, allowing us to extract the initial and final lengths of the spindle and its rate of elongation. We also measured centrosome size, the length of the embryo, and the position of the division plane. The scale bars represent 10 μm (first and third panels) and 2 μm (second panel).

changes in the spindle remains unknown and, similarly, it is also unknown how changes in spindle morphology and dynamics might influence fitness.

Here we present a systematic study of the evolution of the first mitotic spindle in nematodes. We developed a high-throughput imaging platform capable of quantitatively measuring spindle morphology and dynamics: the initial length of the spindle, the speed of anaphase, the final length of the spindle, the size of centrosomes, and the position of the division plane. We used this system to determine the extent of within-species variations in spindles, how spindles change over phylogeny, the manner in which spontaneous mutations alter the spindle, and the relationship between the spindle and fitness. We found that the evolution of the aspects of the spindle we studied can be explained by the combination of the measured effects of spontaneous mutations and stabilizing selection on cell size, quantitatively accounting for both the levels of within-species variation in the spindle and its diversity over ~100 million years of evolution. Our results argue that natural selection acts predominantly on cell size and only indirectly influences the spindle through the scaling of the spindle with cell size. Furthermore, we have discovered that there is extensive within-species genetic variation for spindle morphology and dynamics, which may have implications for human disease and provides a novel route for further mechanistic studies of the spindle and possibly other aspects of cell biology.

Results

Spindles Show Extensive Variation between *Caenorhabditis elegans* Natural Isolates

We first sought to determine the level of within-species variation in spindles, which is currently unknown due to the lack of high-throughput quantitative techniques capable of measuring such diversity. We thus developed a high-throughput imaging platform to study the first mitotic division in *Caenorhabditis elegans*, consisting of 3D time-lapse differential interference contrast microscopy of multiple embryos (Figure 1A) and automated image analysis of the embryo and spindle (Figure 1B) (see the Experimental Procedures for details). This system enabled us to track the pole-to-pole distance of the spindle over time (Figure 1C) and measure the initial length of the spindle, the speed of spindle elongation, and the final length of the spindle, as well as the size of the centrosomes, the position of the division plane, and the length of the embryo.

We used this imaging platform to investigate the extent of within-species variation of spindles by studying 97 *C. elegans* natural isolates (20–40 embryos per isolate) collected from around the world. We found that the differences in spindles between isolates are greater than the differences between embryos from the same isolate (Figures 2A–2C). We observed extensive variation for all aspects of spindles (see Figure S1), as illustrated in Figure 2D for centrosome size, which varies nearly 2-fold across different *C. elegans* natural isolates. The variations between embryos from the same isolate are caused by non-genetic factors, as they are clones. We sought to quantify the contribution of genetic factors to spindle variation, because evolution is caused by changes in the genetic composition of populations. We used H2boot [26], a bootstrapping program (see the Experimental Procedures for details), to decompose the measured phenotypic variance for each trait (V_p) into a genetic component (V_g), namely the variance due to difference between isolates, and an environmental component (V_e), namely the variance between embryos from the same isolate. We found significant genetic variance (V_g) for all traits we studied (Table S1). Thus, there is substantial standing genetic variation for spindle diversity in *C. elegans*.

The traits we measured are not independent of each other; for example, the final length of the spindle is greater in larger embryos (Figure 2E). We used H2boot to determine the partial correlation between pairs of traits, that is, the relation between traits controlling for the influence of other traits. We found significant partial correlations between many traits (Figure 2F). All traits have a significant partial correlation with embryo size (Figure 2F): larger embryos tend to have larger centrosomes and larger spindles, which elongate faster, and a resulting

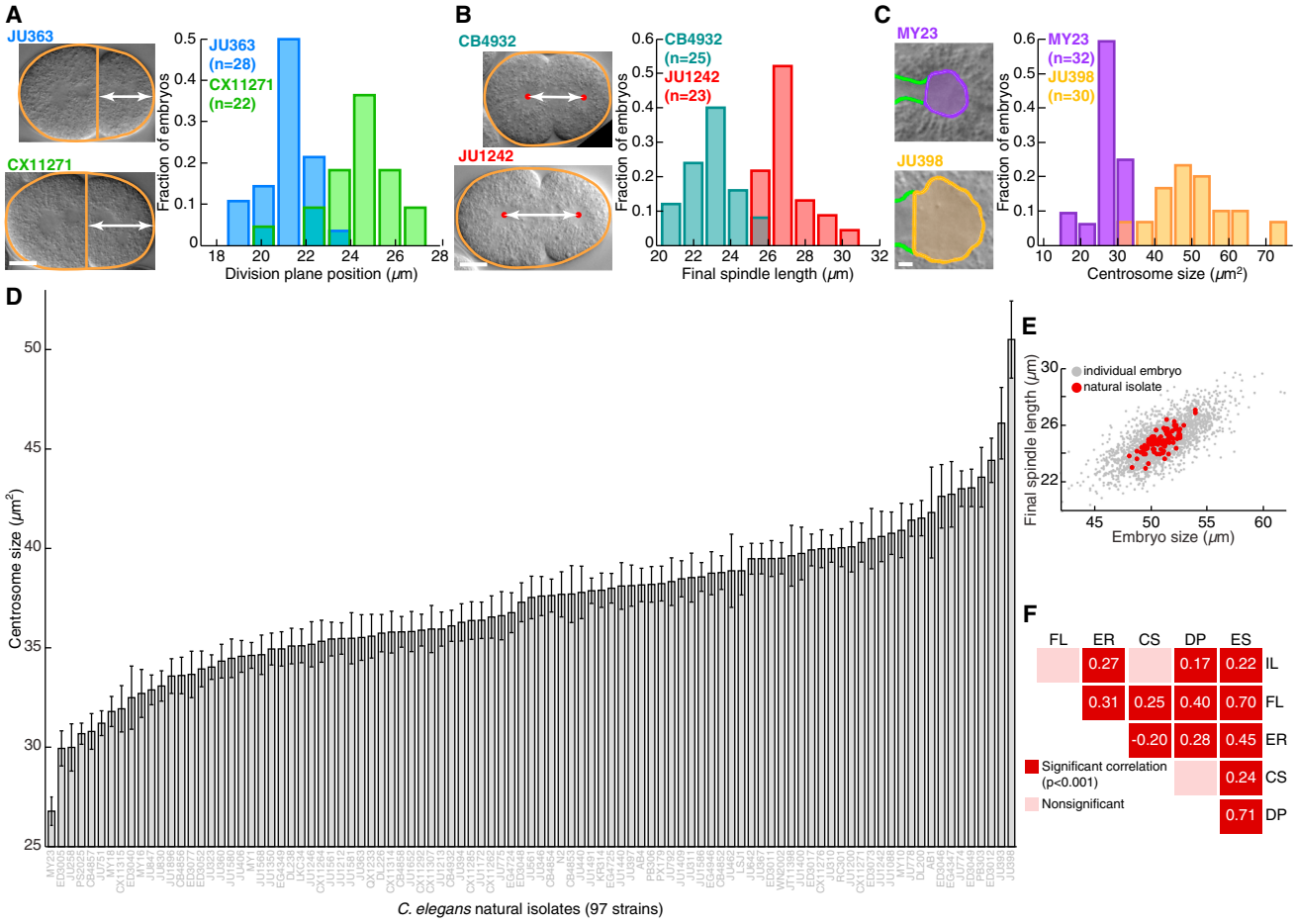

Figure 2. Variation of Spindles across Different *C. elegans* Natural Isolates

(A) Left: representative images showing the position of the division plane in two natural isolates (JU363 and CX11271). Right: histograms of the division-plane position for all embryos measured from these natural isolates. The scale bar represents 10 μm.

(B) Left: representative images showing the final spindle length for two natural isolates (CB4932 and JU1242). Right: histograms of the final spindle length for all embryos measured from these natural isolates. The scale bar represents 10 μm.

(C) Left: representative images of centrosomes in two natural isolates (MY23 and JU398). Right: histograms of centrosome size for all embryos measured from these two isolates are shown. The scale bar represents 2 μm.

(D) Ranked-order plot of centrosome size of the 97 *C. elegans* natural isolates analyzed in this study. Centrosome size varies 2-fold across different isolates.

(E) Plotting final spindle length versus embryo size reveals a correlation between these two variables. Gray dots are values for individual embryos, and red dots are average values for each natural isolate.

(F) Significant ($p < 0.001$) partial correlations between pairs of cell-division traits across *C. elegans* natural isolates: initial spindle length (IL), final spindle length (FL), spindle elongation rate (ER), centrosome size (CS), division-plane position (DP), and embryo size (ES). All traits are correlated with embryo size. See also Figure S1.

division plane farther from the posterior end of the embryo. Because embryo size and cell size are the same for the first mitotic division, this result indicates that all aspects of the spindle we studied scale with cell size.

Spontaneous Mutation Significantly Changes Spindle Morphology and Dynamics

We next studied the processes that give rise to the observed genetic variation for spindles in *C. elegans*. Because all genetic variation ultimately originates from spontaneous mutations, we first investigated how spontaneous mutations influence the spindle. The most direct method of studying the effects of spontaneous mutations on any phenotypic trait is through the use of mutation accumulation (MA) lines, which were generated by propagating randomly chosen single progeny for ~250 generations (see Figure S2) [27]. This procedure results in the MA lines having an effective population size of one, allowing the accumulation of non-lethal and non-sterile mutations during their production. The manner in which spontaneous mutations perturb the spindle can be determined by measuring the divergence in spindles between the MA lines. We imaged cell division in 94 MA lines (20–40 embryos per line, generated from two different isolates, N2 and PB306). All spindle traits significantly varied among the MA lines, and the variance of these traits in the MA lines was greater than the variance in the ancestral generation (as illustrated for the elongation rate of the spindle in Figure 3A), indicating a significant effect of spontaneous mutations on spindles. Whereas the variance of the traits across the MA lines was greater than in the ancestral generation, the mean of the traits across the MA lines did not significantly change ($p < 0.05$ by F test), arguing that spontaneous mutations are as likely to produce

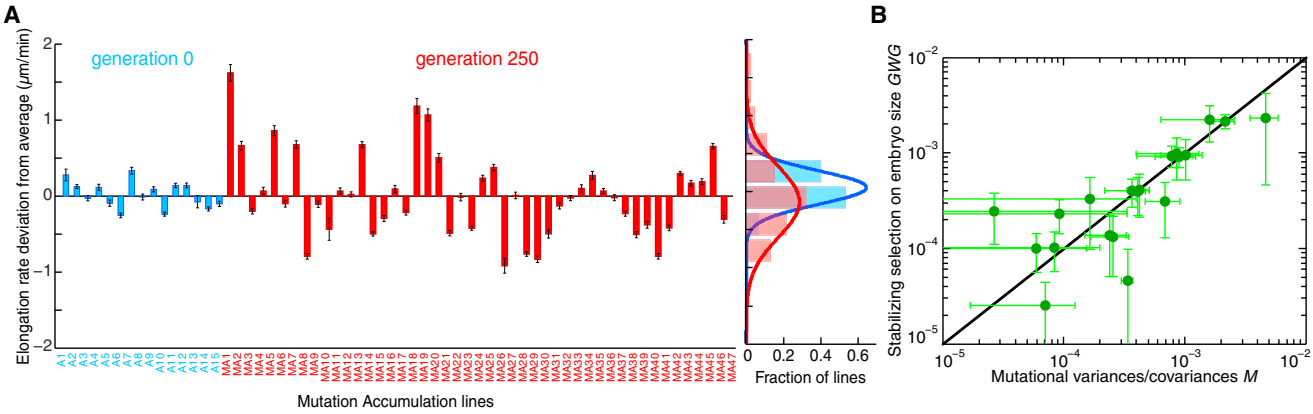

Figure 3. Stabilizing Selection on Embryo Size Quantitatively Predicts within-Species Variation of Spindle Traits

(A) Effect of spontaneous mutations on spindles. Deviation of spindle elongation rate from the average of the ancestral lines at generation zero (blue) and after 250 generations of mutation accumulation (red). Error bars indicate the SE. Histograms of the deviations are shown in the right-hand panel. Solid lines indicate Gaussian fits to these distributions.

(B) Stabilizing selection on embryo size quantitatively explains variation of cell-division traits. Each element of the matrix M, the variance/covariance matrix of the effect of spontaneous mutations on spindle traits measured in the MA lines, is plotted against the corresponding element of the matrix GWG, where G is the variance/covariance matrix of traits measured across *C. elegans* natural isolates and W is the matrix of selection coefficients, which has only one non-zero element related to the strength of stabilizing selection on embryo size. The points predominantly fall along the unitary line (black), indicating consistency with the equation $M = GWG$ (see text). Error bars indicate SEs measured by bootstrapping.

See also Figure S2.

increases as decreases in these traits (see Table S1). The variations between embryos from the same MA line are caused by non-genetic factors, as they are clones, whereas differences between different MA lines are due to genetic factors: random mutations that accumulated during the generation of each line. We used H2boot to extract the genetic component of the variance of the traits in the MA lines, that is, the variance that can be attributed to the difference between MA lines. We then used these results to determine the amount of genetic variance generated by spontaneous mutations in a single generation (V_m) for each trait (see Table S1).

Having quantified the effects of spontaneous mutations, we could evaluate the validity of different scenarios for the evolution of the spindle in *C. elegans*. For a neutral trait with evolutionary dynamics governed only by drift, the ratio of V_g, measured across natural isolates, to the mutational variance (V_m), measured in the MA lines, is four times the effective population size (N_e) [12], estimated to be ~10,000 in *C. elegans* from molecular approaches [28] (i.e., $V_g/V_m = 4\ N_e$ ~40,000 for neutral drift). All the traits we studied show less genetic variation than expected from neutral drift, with embryo size showing the greatest deviation from neutral expectation (V_g/V_m ~250 for embryo size and V_g/V_m ~370–1,400 for other traits), allowing the neutral drift model to be strongly rejected ($p < 0.001$ by bootstrapping). Thus, we conclude that variations in the aspects of the spindle we studied are not determined solely by neutral drift.

Stabilizing Selection on Embryo Size Quantitatively Explains the within-Species Variations in Spindles

The observed deviations from neutral expectations might be due to the influence of selection. Hypothetically, spindles could be locally adapted to the natural environment of each of the isolates, but the observation that the level of local genetic diversity is similar to the extent of global variation [28] and lack of population structure in *C. elegans* [28], and the absence of correlation between spindle traits and the location (see Figures S3A and S3B) or temperature (Figures S3C and S3D) from where isolates were collected, argues against this scenario. An alternative possibility is that there is a single optimal behavior of the spindle in *C. elegans*, and that the diversity across the isolates is due to a balance between spontaneous mutations continually generating new variations and stabilizing selection preferentially eliminating less fit individuals with spindles that deviate from the optimum. Such a mutation-stabilizing selection balance has long been considered to be one of the primary processes that maintains standing genetic variation for quantitative traits [29]. Indirect support for this scenario comes from the observation that crossing two of the natural isolates produces offspring with more extreme (transgressive) values of the cell-division traits than the parental lines (data not shown), suggesting prevalent compensatory substitutions.

We sought to further explore the validity of mutation-stabilizing selection balance for the spindle by testing whether the observed levels of standing genetic variation for spindle traits can be explained by the measured effects of spontaneous mutations and the proposed role of stabilizing selection. Because the measured spindle traits are correlated with each other and with embryo size, it is possible that stabilizing selection might directly act on only a subset of these traits and indirectly influence the other traits through their mutual correlations [30]. Because embryo size shows the greatest deviation from neutral expectations (see above) and is correlated with all spindle traits we measured (Figure 2F), we wondered whether stabilizing selection acting solely on embryo size is sufficient to account for the level of genetic variation of spindle traits in *C. elegans*. For a set of traits subject to mutation-stabilizing selection balance [31],

$$M = GWG, \qquad \text{(Equation 1)}$$

where M is a symmetric matrix with diagonal elements of genetic mutational variances generated per generation (V_m for

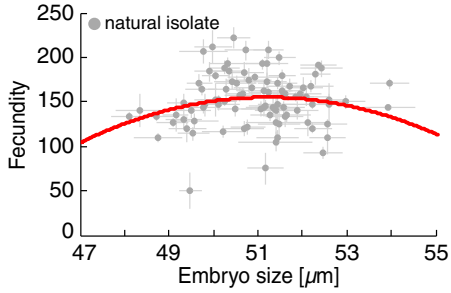

Figure 4. Fecundity Is Quadratically Correlated with Embryo Size

Fecundity (see the Experimental Procedures for details) as a function of embryo size in the natural isolates. Gray dots are values for individual isolates (mean ± SE). The red line shows a quadratic fit to the data (see the Experimental Procedures for details). See also Figure S3.

each trait) and off-diagonal elements of genetic mutational covariances between pairs of spindle traits (calculated by multivariate ANOVAs; see the Experimental Procedures for details and Table S2, part B). The symmetric matrix *G* has diagonal elements of genetic variances among the natural isolates (V_g for each trait) and off-diagonal elements of the genetic covariances between pairs of traits in the natural isolates (calculated by multivariate ANOVAs; see the Experimental Procedures for details and Table S2, part A). *W* is a matrix describing the pattern and strength of stabilizing selection on the traits. We postulated stabilizing selection solely on embryo size by setting all elements of *W* to zero except for the one corresponding to embryo size (w_{ES} = 0.007 μm^{-2}), and checked the validity of Equation 1 by plotting the matrix elements of *M* versus the matrix elements of *GWG* (Figure 3B). These matrix elements lie along a straight line (Figure 3B), demonstrating consistency with Equation 1 and showing that stabilizing selection on embryo size, and the correlations of the spindle with embryo size, is sufficient to account for the within-species variations in *C. elegans* for all aspects of spindles we studied.

To further test for the existence of stabilizing selection on embryo size, we measured fecundity in the *C. elegans* natural isolates (see the Experimental Procedures for details) and found that, among all aspects of cell division we studied, the strongest association was with embryo size: embryo size is quadratically correlated with fecundity ($p < 0.003$; see Figure 4), with an optimal embryo size of 51 ± 1 μm (mean ± SD) and a deviation of 1 μm leading to a reduction in fecundity of ~2%. This strength of stabilizing selection inferred from the quadratic regression on fecundity is similar in magnitude to that estimated by comparing the levels of mutational and standing genetic (co)variances through the use of Equation 1. The agreement between these two different measurements further supports the existence of stabilizing selection on embryo size. Thus, there is strong evidence for stabilizing selection on embryo size in *C. elegans*, and the combination of this stabilizing selection with the measured effects of spontaneous mutations and the correlation of spindle traits with embryo size are sufficient to quantitatively explain the extent of within-species variation of spindles in *C. elegans*.

Stabilizing Selection on Embryo Size Quantitatively Explains the between-Species Variations in Spindles

The *C. elegans* population has experienced recent chromosome-scale selective sweeps leading to reduced genetic diversity and extensive linkage disequilibrium [28]. Because these processes could also affect standing genetic variation for spindles, we investigated the extent of spindle variation in other species with different population dynamics. We imaged 19 natural isolates of *C. briggsae*, 16 natural isolates of *C. brenneri*, and 13 natural isolates of *C. remanei*, and found that the within-species genetic variances of cell-division traits (Figure 5A), and the pattern of correlations between them (Figure 5B), in the other species are very similar to those in *C. elegans*. This argues that the level of genetic variance for spindle traits and embryo size is not caused by the specific sweeps that occurred in *C. elegans*, or the particular pattern of linkage disequilibrium, which is expected to be different in these species with different mating types (androdiecious for *C. elegans* and *C. briggsae*, gonochoristic for *C. brenneri* and *C. remanei*), and is consistent with our inference of stabilizing selection.

We next studied cell division in 37 additional species of nematodes, thought to span ~120 million years of evolution [32]. These species display a range of embryo sizes and spindle behaviors (Figure 5C). Because the extent and pattern of within-species variations in spindles can be explained by the combination of stabilizing selection on embryo size and the correlation of spindle traits with embryo size, we wondered whether the same mechanism could also account for the diversity of spindles across different species of nematodes that we studied. We first considered the dynamics of evolutionary changes of embryo size and found that the divergence of embryo size with phylogenetic distance cannot be explained by neutral drift or stabilizing selection with a single optimum but is consistent with each species having its own optimal size (see the Experimental Procedures and Figure S4).

We next investigated whether differences in optimal embryo size could account for the diversity of spindle traits in these different species. Quantitative genetic theory predicts that if natural selection acts on one trait (i.e., embryo size) it will drive changes in correlated traits (i.e., final spindle length, centrosome size, and the spindle traits we studied), with a response in the correlated trait proportional to the genetic covariance between the traits [12]. Therefore, for species with similar genetic variances and covariances between traits (as is the case for the nematodes studied here; Figures 5A and 5B), the change in the mean of the correlated traits across species is predicted to be linearly proportional to the change in the mean of the selected trait (i.e., embryo size), with a regression coefficient equal to the ratio of genetic covariance of the selected and correlated traits divided by the genetic variance of the selected trait (see [33] and the Experimental Procedures for details). Thus, to test the validity of an evolutionary scenario in which embryo size is subject to stabilizing selection with an optimal embryo size that varies between species and differences in spindle traits are caused by their correlated response to selection on embryo size, we measured the regression between embryo size and spindle traits across species and compared these results with predictions from quantitative genetic theory based on the patterns of within-species variation in spindle traits measured in *C. elegans*. The predictions of this model, which has no free parameters, show quantitative agreement for all aspects of spindles we studied (Figure 5D). Therefore, stabilizing selection on embryo size, indirectly influencing the spindle through its correlation with embryo size, is sufficient to quantitatively explain the differences in spindles between species of nematodes.

Please cite this article in press as: Farhadifar et al., Scaling, Selection, and Evolutionary Dynamics of the Mitotic Spindle, Current Biology (2015), http://dx.doi.org/10.1016/j.cub.2014.12.060

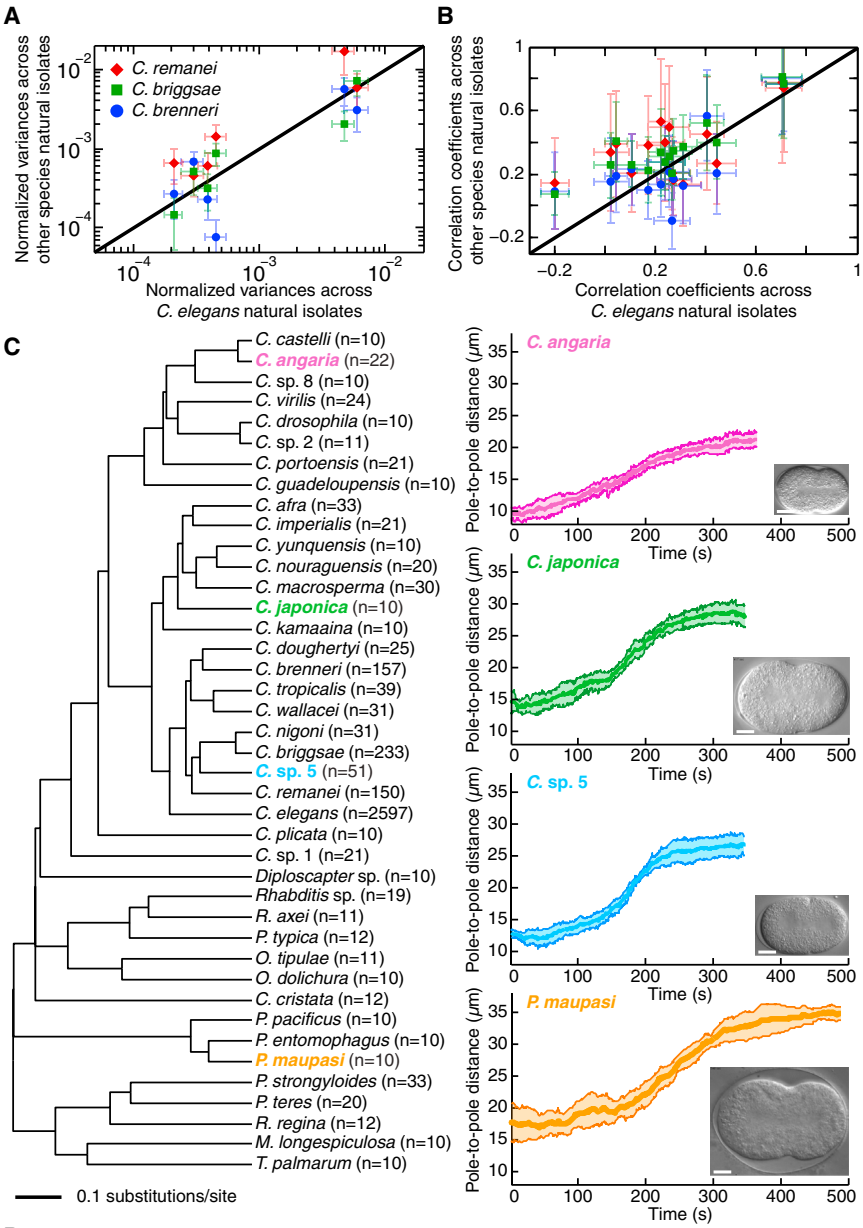

regression on embryo size across species

	predicted	measured
Initial length	0.14 ± 0.04	0.20 ± 0.06
Final length	0.55 ± 0.05	0.57 ± 0.10
Elongation rate	0.21 ± 0.05	0.15 ± 0.08
Centrosome size	1.67 ± 0.49	1.55 ± 0.64
Division plane	0.51 ± 0.04	0.46 ± 0.04

Figure 5. Stabilizing Selection on Embryo Size Quantitatively Predicts between-Species Variation of Spindle Traits

(A and B) Variances of the measured traits, normalized by the species mean (A), and correlation coefficients between the traits (B) in *C. remanei*, *C. briggsae*, and *C. brenneri* plotted against the variances or covariances of the corresponding traits in *C. elegans* (±SE). The variances and covariances predominantly fall along the unitary line (black), indicating that the pattern of within-species variation for these traits in the three other nematode species is similar to that in *C. elegans*.

(C) Characterization of the first cell division in 41 species of nematodes with known phylogeny. Pole-to-pole distances as a function of time are plotted for four sample species (the solid line indicates the mean, and the shaded region indicates the SD measured for multiple embryos). The scale bars represent 10 μm.

(D) A model, with no free parameters, in which spindle traits scale with embryo size as they do in *C. elegans* and embryo size is subject to stabilizing selection with a different optimum for each species is sufficient to explain between-species variation of these traits. Blue dots (mean ± SE) show spindle final length and the position of the division plane relative to embryo size for the different species. The red line is the prediction of the stabilizing selection model, and the green line is fit to the data. The table compares predicted coefficients of regression for different spindle traits with measured ones. Errors on predicted regression coefficients were calculated by bootstrapping (see the Experimental Procedures for details).

See also Figure S4.

Discussion

Taken together, our results show that the effects of spontaneous mutations on cell division in a single generation, combined with stabilizing selection on embryo size, are sufficient to quantitatively explain the levels of variation in the spindle within species and over ~100 million years of evolution. Our data argue that selection acts predominantly on cell/embryo size and only indirectly influences the spindle through the scaling of the spindle with cell size.

Previous work has shown that spindles scale with cell size over the course of early development [18, 34–40]. Thus, the scaling of the spindle with cell size drives its variation over both ontogeny and phylogeny. It will be interesting to investigate whether common mechanisms account for the scaling of the spindle with cell size in these different contexts.

Although all the aspects of the spindle we studied are correlated with cell size, these traits are only partially determined by cell size: for example, the partial correlation between cell size and initial spindle length is only 0.22 (Figure 2F). This observation is consistent with the knowledge that many factors unrelated to cell size contribute to spindle length, such as microtubule polymerization dynamics and the activity of motor proteins [15, 16]. The limited correlations of the spindle with cell size, along with stabilizing selection on cell size, are still sufficient to determine the nature and extent of within-species variation in spindles and their changes across nematode species.

The correlated response to selection on cell size cannot explain all variations in spindles across all Eukaryotes, as

spindles in distantly related organisms with similar cell sizes have different morphologies and sizes and different interactions with the nuclear envelope, and vary in other ways [4, 5, 15, 16]. However, we speculate that similar principles to those found in this study may apply in other systems: that many aspects of variation in spindles may be driven by their correlated responses to other traits under selection. The response of correlated traits, particularly the correlation of traits with body size, has been a major focus of study of evolution at the organismal level [12, 30, 33] and might be of similar general importance for evolution at the subcellular level. For the nematodes we studied, their cell size during the first mitotic division is the same as their size at birth. Extensive evidence demonstrates that size at birth is subject to stabilizing selection in a wide variety of species [41], consistent with our inference of stabilizing selection on cell size during the first mitotic division in nematodes. Different selective pressure may dominate in other contexts, driving different correlated evolutionary changes in spindles. The presence of significant within-species standing genetic variation for spindles and the observation that spontaneous mutations can rapidly modify spindles show that they have a broad capacity for such evolutionary changes.

Our finding of extensive within-species variation for spindles demonstrates that the "wild-type" behavior of spindles encompasses a surprisingly broad range. Evolutionary studies have consistently found within-species variation for nearly all attributes at the organismal level [12], and our observations indicate that similar variation exists at the cell biological level. This suggests caution in making generalizations about cell biology from studies performed on only a single natural isolate or highly inbred lab strain. The existence of within-species variation is not only important for understanding the evolution of cellular traits, like we have shown here, it also opens novel possibilities for the study of mechanistic aspects of cell biology by allowing the application of powerful approaches from quantitative genetics to map the genetic basis of this variation and to differentiate correlative and causative relationships between traits [42]. Within-species genetic diversity is greater in humans than *C. elegans* [43], suggesting that humans may display even larger variations in cell biological behaviors, which may have implications for disease.

Experimental Procedures

Maintenance and Time-Lapse Differential Interference Contrast Microscopy of *C. elegans* Strains

We cultured all *C. elegans* strains at 24°C on nematode growth media (NGM) plates and fed with *Escherichia coli* OP50 as described previously [44]. We dissected adult worms in M9 buffer, mounted embryos on a 4% agar pad between a slide and a coverslip, and used an eyelash to position multiple embryos in close proximity. Differential interference contrast (DIC) microscopy was performed on a Nikon Eclipse TE2000-E microscope equipped with a 60× Plan Apochromat NA 1.2 objective and an oil-immersed condenser NA 1.4. We acquired seven images every 0.5 s with a Hamamatsu ORCA-R2 camera, and used a piezo-driven nanopositioning Physik Instrumente E-709 to cover a volume of ~3 μm at steps of 0.5 μm during this interval.

Maintenance and Time-Lapse DIC Microscopy of Other Nematode Strains

We cultured strains other than *C. elegans* at 20°C on NGM plates and fed with *E. coli* OP50 as described previously [44]. We dissected adult worms in M9 buffer and mounted the embryos on 2% agarose pads. We used DIC microscopy to image the first embryonic division every 0.5 s with a Zeiss Axio Imager A2 microscope equipped with a 100× Plan Apochromat NA 1.4 objective and a digital Kappa camera (DX4-285FW).

Image Processing and Quantification of Cell-Division Traits

We developed custom-designed image-processing software as described [45] to track spindle pole-to-pole distance in DIC images of *C. elegans* embryos from formation of the mitotic spindle upon completion of the first division. For those embryos that the automated tracking failed, we manually tracked spindle poles. For each embryo, we measured pole-to-pole distance as a function of time and fitted a sigmoid function $l(t) = l_0 + l_1/(1 + \exp(-(t - t_0)/\tau))$ to the data. We defined initial spindle length as l_0, final spindle length as $(l_0 + l_1)$, and elongation rate as $l_1/4\tau$. t_0 is the time at which the spindle is halfway between its initial and final lengths. We defined centrosome size as the average size of centrosomes for $t > t_0 + e\tau$. We manually measured embryo size as the distance between the anterior and posterior ends of the cortex upon formation of the new cleavage furrow, when ruffling of the cortex is minimal, and the division-plane position as the distance of the cleavage furrow from the posterior cortical end of the embryo at the end of cell division. For all strains other than *C. elegans*, we manually determined the initial spindle length, final spindle length, and rate of elongation from the pole-to-pole distance curves of each embryo.

Estimation of Variances, Covariances, and Correlations of Cell-Division Traits

We used H2boot [26], a bootstrapping software for analysis of multivariate quantitative genetic data, to measure variances and covariances of cell-division traits as well as partial correlation coefficients between pairs of traits. We used the "one-way ANOVA among RI lines" option with 10,000 bootstrapping runs, and standardized trait values of each embryo by subtracting from the average and dividing by the SD calculated for all embryos of the data set. We then used the SD of the traits to calculate variances and covariances with physical units. To calculate the mutational variances per generation (V_m) for each trait, we subtracted the among-line variance measured at generation zero from the among-line variance measured at generation 250 and divided by 250, the total number of mutation accumulation generations. We measured the per-generation mutational matrix of variances and covariances (M) by subtracting the among-line variance-covariance matrix measured at generation zero from the among-line variance-covariance matrix measured at generation 250 and dividing by 250.

Estimating the Change in the Mean of Cell-Division Traits in the MA Lines

The difference in trait means between the generation zero (G0) ancestor and the MA lines was assessed by solving the general linear model

$$Y = Treatment + Line(Treatment) + Replicate(Line(Treatment)),$$

where Y is the trait value, *Treatment* (MA or G0) is a fixed effect, and *Line* (G0 pseudoline or MA line) and *Replicate* are random effects. Variance components were estimated by restricted maximum likelihood separately for G0 and MA treatments. Significance was determined by F tests using type III sums of squares. Degrees of freedom were determined using the Kenward-Roger method [46]. Analyses were performed using the MIXED procedure in SAS version 9.4.

Fecundity Measurements for the *C. elegans* Natural Isolates

Animals were grown in 96-well microtiter plates with 50 μl of S medium and HB101 bacterial food in each well. One mid-to-late fourth larval stage animal was singled out using platinum wire to each well. Animals were grown for 72 hr in these conditions and the number of offspring per well was measured on the COPAS BIOSORT (Union Biometrica). We fitted a quadratic function, $F = -(E - E_0)^2/\omega^2 + \eta$, to the data measured across *C. elegans* natural isolates, where F and E indicate fecundity and embryo size, respectively, E_0 is the optimal embryo size, and ω is the strength of stabilizing selection. We measured the fit parameters for standardized fecundity (divided by the average fecundity of the natural isolates) and standardized embryo size (subtracted and then divided by the average embryo size of the natural isolates), and then scaled them to their relative values (E_0 = 51 μm, ω = 0.6 μm^{-1}). We calculated the significance of the quadratic model by contrasting it with a model where fecundity has no relation with embryo size.

Phylogeny Construction of Nematode Species

We sequenced several portions of the gene encoding RNA polymerase II from *Pristionchus entomophagus*, *P. maupasi*, and *Oscheius dolichura*. These sequences were added to the previously published sequences [6, 47] from other species and a maximum-likelihood phylogram was constructed as described before [47].

Comparative Analysis of Spindle Traits and Embryo Size in Different Species of Nematodes

We investigated the dynamics of evolutionary changes of embryo size by comparing the predictions of three different models for the divergence of embryo size with phylogenetic distance across the species we studied. For each pair of species, we calculated the square of the difference in embryo size and the approximate phylogenetic distance measured by the substitutions/site in RNA polymerase II, converted to generations using an estimated 200 million generations separating *C. elegans* and *C. briggsae* (see [32]). We then averaged over species of similar phylogenetic distances and compared with the prediction of three evolutionary models for the divergence of embryo size (Figure S4): neutral drift, stabilizing selection with one optimal embryo size, and stabilizing selection with multiple optimal embryo sizes.

The neutral drift model predicts that the divergence in embryo size increases linearly with generation number as $V_{gES}t/N_e$ (see [48, 49] for details), where $V_{gES} = 0.55\ \mu m^2$ (see Table S1) and $N_e = 10{,}000$ [28]. The neutral drift model is clearly inconsistent with the data, as it predicts that embryo size should diverge hundreds of times faster than observed (Figure S4).

The stabilizing selection model with one optimal embryo size predicts a linear divergence for embryo size for short evolutionary timescales, which converges to a constant value on longer timescales as described by $V_{gES}(1-\exp(-2st))/2sN_e$ (see [48, 49]). Here $s = V_{mES}/V_{gES}$, which is the ratio of the per-generation variance produced by spontaneous mutations for embryo size, and its additive genetic variance indicates the strength of stabilizing selection on embryo size. Using the values for $V_{mES} = 2.17\times10^{-3}\mu m^2$ and $V_{gES} = 0.55\ \mu m^2$ from our measurements in *C. elegans* (see Table S1), the stabilizing selection model with one optimal embryo size predicts that divergence in embryo size should not increase with phylogenetic distance across the species that we studied, which strongly deviates from observations (Figure S4).

We next considered the model of stabilizing selection with multiple optimal embryo sizes. The simplest model is to assume that the optimum embryo size varies over phylogeny with Brownian dynamics, in which case the divergence in embryo size is $\alpha t + V_{gES}(1-\exp(-2st))/2sN_e$ (see [48, 49]). Here, α characterizes how the optimal embryo size varies over phylogeny, which could be due to the dynamics of changes in the ecological niches of the species. A best fit gives $\alpha = 5.8\times10^{-7}\ \mu m^2$, and is consistent with the divergence of embryo size across the species we studied (see Figure S4). A more complex model of the movement of the optimum might better capture the details of the dynamics of the divergence of embryo size, but even the highly simplified Brownian model correctly captures the evolutionary trends.

Given stabilizing selection on embryo size with different optimal values for other nematode species we studied and a linear relation between spindle traits and embryo size, we predicted the slope of the linear regression from our measurements in *C. elegans*. The slope of the regression is $G_{i,ES}/G_{ES,ES}$ (see [33] for details), where $G_{i,ES}$ is the genetic covariance of trait i and embryo size (ES), and $G_{ES,ES}$ is the genetic variance of embryo size measured in *C. elegans*. We measured the regression slope and the SE with bootstrapping.

Supplemental Information

Supplemental Information includes four figures and two tables and can be found with this article online at http://dx.doi.org/10.1016/j.cub.2014.12.060.

Author Contributions

R.F., T.M.-R., M.D., and D.J.N. designed the project. R.F. and A.-C.V. performed experiments. R.F. and C.F.B. performed data analysis. E.C.A. performed fitness measurement. R.F. and D.J.N. wrote the manuscript.

Acknowledgments

We thank Bodo Stern and Annalise Paaby for comments. We thank Asher Cutter, Dee Denver, M.A. Félix, Karin Kiontke, Ralf Sommer, and the Caenorhabditis Genetics Center (CGC) for providing us with some strains used in this study. The CGC is funded by the NIH Office of Research Infrastructure Programs (P40 OD010440). We also thank Theresa Grana for providing the *Rhabditis* species TMG33 strain. We thank Karin Kiontke for help in phylogenetic tree reconstruction. The computations in this paper were run on the Odyssey cluster supported by the FAS Division of Science, Research Computing Group at Harvard University. Support was provided by NIH grant R01GM072639 to C.F.B., Deutsche Forschungsgemeinschaft grant MU1423/3-2 (SPP 1384) to T.M.-R., and Human Frontier Science Program grant RGP 0034/2010 to T.M.-R., M.D., and D.J.N.

Received: November 6, 2014
Revised: December 24, 2014
Accepted: December 24, 2014
Published: February 12, 2015

References

1. Wilson, K.L., and Dawson, S.C. (2011). Evolution: functional evolution of nuclear structure. J. Cell Biol. *195*, 171–181.
2. Mowbrey, K., and Dacks, J.B. (2009). Evolution and diversity of the Golgi body. FEBS Lett. *583*, 3738–3745.
3. Carvalho-Santos, Z., Azimzadeh, J., Pereira-Leal, J.B., and Bettencourt-Dias, M. (2011). Evolution: tracing the origins of centrioles, cilia, and flagella. J. Cell Biol. *194*, 165–175.
4. Kubai, D.F. (1975). The evolution of the mitotic spindle. Int. Rev. Cytol. *43*, 167–227.
5. Heath, I.B. (1980). Variant mitoses in lower eukaryotes: indicators of the evolution of mitosis. Int. Rev. Cytol. *64*, 1–80.
6. Brauchle, M., Kiontke, K., MacMenamin, P., Fitch, D.H.A., and Piano, F. (2009). Evolution of early embryogenesis in rhabditid nematodes. Dev. Biol. *335*, 253–262.
7. Alon, U. (2006). An Introduction to Systems Biology: Design Principles of Biological Circuits (Boca Raton: Chapman & Hall/CRC Mathematical and Computational Biology).
8. Mast, F.D., Barlow, L.D., Rachubinski, R.A., and Dacks, J.B. (2014). Evolutionary mechanisms for establishing eukaryotic cellular complexity. Trends Cell Biol. *24*, 435–442.
9. Lynch, M. (2007). The Origins of Genome Architecture (Sunderland: Sinauer).
10. Karsenti, E. (2008). Self-organization in cell biology: a brief history. Nat. Rev. Mol. Cell Biol. *9*, 255–262.
11. Cavalier-Smith, T. (2010). Origin of the cell nucleus, mitosis and sex: roles of intracellular coevolution. Biol. Direct *5*, 7.
12. Lynch, M., and Walsh, B. (1998). Genetics and Analysis of Quantitative Traits (Sunderland, MA: Sinauer).
13. Harvey, P.H., and Pagel, M.D. (1991). The Comparative Method in Evolutionary Biology (New York: Oxford University Press).
14. Hartl, D.L., and Clark, A.G. (2007). Principles of Population Genetics (Sunderland: Sinauer).
15. Helmke, K.J., Heald, R., and Wilbur, J.D. (2013). Interplay between spindle architecture and function. Int. Rev. Cell Mol. Biol. *306*, 83–125.
16. Goshima, G., and Scholey, J.M. (2010). Control of mitotic spindle length. Annu. Rev. Cell Dev. Biol. *26*, 21–57.
17. Gan, L., Ladinsky, M.S., and Jensen, G.J. (2011). Organization of the smallest eukaryotic spindle. Curr. Biol. *21*, 1578–1583.
18. Wühr, M., Chen, Y., Dumont, S., Groen, A.C., Needleman, D.J., Salic, A., and Mitchison, T.J. (2008). Evidence for an upper limit to mitotic spindle length. Curr. Biol. *18*, 1256–1261.
19. Helmke, K.J., and Heald, R. (2014). TPX2 levels modulate meiotic spindle size and architecture in *Xenopus* egg extracts. J. Cell Biol. *206*, 385–393.
20. Loughlin, R., Wilbur, J.D., McNally, F.J., Nédélec, F.J., and Heald, R. (2011). Katanin contributes to interspecies spindle length scaling in *Xenopus*. Cell *147*, 1397–1407.
21. Brown, K.S., Blower, M.D., Maresca, T.J., Grammer, T.C., Harland, R.M., and Heald, R. (2007). *Xenopus tropicalis* egg extracts provide insight into scaling of the mitotic spindle. J. Cell Biol. *176*, 765–770.
22. Hellsten, U., Khokha, M.K., Grammer, T.C., Harland, R.M., Richardson, P., and Rokhsar, D.S. (2007). Accelerated gene evolution and subfunctionalization in the pseudotetraploid frog *Xenopus laevis*. BMC Biol. *5*, 31.
23. Evans, B.J., Kelley, D.B., Tinsley, R.C., Melnick, D.J., and Cannatella, D.C. (2004). A mitochondrial DNA phylogeny of African clawed frogs: phylogeography and implications for polyploid evolution. Mol. Phylogenet. Evol. *33*, 197–213.
24. Wickstead, B., and Gull, K. (2006). A "holistic" kinesin phylogeny reveals new kinesin families and predicts protein functions. Mol. Biol. Cell *17*, 1734–1743.
25. Wickstead, B., and Gull, K. (2007). Dyneins across eukaryotes: a comparative genomic analysis. Traffic *8*, 1708–1721.

26. Phillips, P.C. (2002). H2boot: bootstrap estimates and tests of quantitative genetic data. http://darkwing.uoregon.edu/~pphil/software.html.
27. Baer, C.F., Shaw, F., Steding, C., Baumgartner, M., Hawkins, A., Houppert, A., Mason, N., Reed, M., Simonelic, K., Woodard, W., and Lynch, M. (2005). Comparative evolutionary genetics of spontaneous mutations affecting fitness in rhabditid nematodes. Proc. Natl. Acad. Sci. USA *102*, 5785–5790.
28. Andersen, E.C., Gerke, J.P., Shapiro, J.A., Crissman, J.R., Ghosh, R., Bloom, J.S., Félix, M.-A., and Kruglyak, L. (2012). Chromosome-scale selective sweeps shape *Caenorhabditis elegans* genomic diversity. Nat. Genet. *44*, 285–290.
29. Bürger, R. (2000). The Mathematical Theory of Selection, Recombination, and Mutation (Chichester: John Wiley & Sons).
30. Lande, R., and Arnold, S.J. (1983). The measurement of selection on correlated characters. Evolution *37*, 1210–1226.
31. Walsh, B., and Lynch, M. (2012). Evolution and selection of quantitative traits. http://nitro.biosci.arizona.edu/zbook/NewVolume_2/newvol2.html.
32. Cutter, A.D. (2008). Divergence times in *Caenorhabditis* and *Drosophila* inferred from direct estimates of the neutral mutation rate. Mol. Biol. Evol. *25*, 778–786.
33. Lande, R. (1979). Quantitative genetic analysis of multivariate evolution, applied to brain: body size allometry. Evolution *33*, 402–416.
34. Courtois, A., Schuh, M., Ellenberg, J., and Hiiragi, T. (2012). The transition from meiotic to mitotic spindle assembly is gradual during early mammalian development. J. Cell Biol. *198*, 357–370.
35. Good, M.C., Vahey, M.D., Skandarajah, A., Fletcher, D.A., and Heald, R. (2013). Cytoplasmic volume modulates spindle size during embryogenesis. Science *342*, 856–860.
36. Greenan, G., Brangwynne, C.P., Jaensch, S., Gharakhani, J., Jülicher, F., and Hyman, A.A. (2010). Centrosome size sets mitotic spindle length in *Caenorhabditis elegans* embryos. Curr. Biol. *20*, 353–358.
37. Hara, Y., and Kimura, A. (2009). Cell-size-dependent spindle elongation in the *Caenorhabditis elegans* early embryo. Curr. Biol. *19*, 1549–1554.
38. Hazel, J., Krutkramelis, K., Mooney, P., Tomschik, M., Gerow, K., Oakey, J., and Gatlin, J.C. (2013). Changes in cytoplasmic volume are sufficient to drive spindle scaling. Science *342*, 853–856.
39. Wilbur, J.D., and Heald, R. (2013). Mitotic spindle scaling during *Xenopus* development by kif2a and importin α. eLife *2*, e00290.
40. Decker, M., Jaensch, S., Pozniakovsky, A., Zinke, A., O'Connell, K.F., Zachariae, W., Myers, E., and Hyman, A.A. (2011). Limiting amounts of centrosome material set centrosome size in *C. elegans* embryos. Curr. Biol. *21*, 1259–1267.
41. Stearns, S.C. (2004). The Evolution of Life Histories (New York: Oxford University Press).
42. Rockman, M.V. (2008). Reverse engineering the genotype-phenotype map with natural genetic variation. Nature *456*, 738–744.
43. Barrière, A., and Félix, M.-A. (2005). Natural variation and population genetics of *Caenorhabditis elegans*. WormBook, 1–19.
44. Brenner, S. (1974). The genetics of *Caenorhabditis elegans*. Genetics *77*, 71–94.
45. Farhadifar, R., and Needleman, D. (2014). Automated segmentation of the first mitotic spindle in differential interference contrast microscopy images of *C. elegans* embryos. In Mitosis: Methods and Protocols, Methods in Molecular Biology, D.J. Sharp, ed. (New York: Springer), pp. 41–45.
46. Kenward, M.G., and Roger, J.H. (1997). Small sample inference for fixed effects from restricted maximum likelihood. Biometrics *53*, 983–997.
47. Kiontke, K.C., Félix, M.-A., Ailion, M., Rockman, M.V., Braendle, C., Pénigault, J.-B., and Fitch, D.H. (2011). A phylogeny and molecular barcodes for *Caenorhabditis*, with numerous new species from rotting fruits. BMC Evol. Biol. *11*, 339.
48. Hansen, T.F., and Martins, E.P. (1996). Translating between microevolutionary process and macroevolutionary patterns: the correlation structure of interspecific data. Evolution *50*, 1404–1417.
49. Estes, S., and Arnold, S.J. (2007). Resolving the paradox of stasis: models with stabilizing selection explain evolutionary divergence on all timescales. Am. Nat. *169*, 227–244.

Current Biology

Supplemental Information

Scaling, Selection, and Evolutionary Dynamics of the Mitotic Spindle

Reza Farhadifar, Charles F. Baer, Aurore-Cécile Valfort, Erik C. Andersen, Thomas Müller-Reichert, Marie Delattre, and Daniel J. Needleman

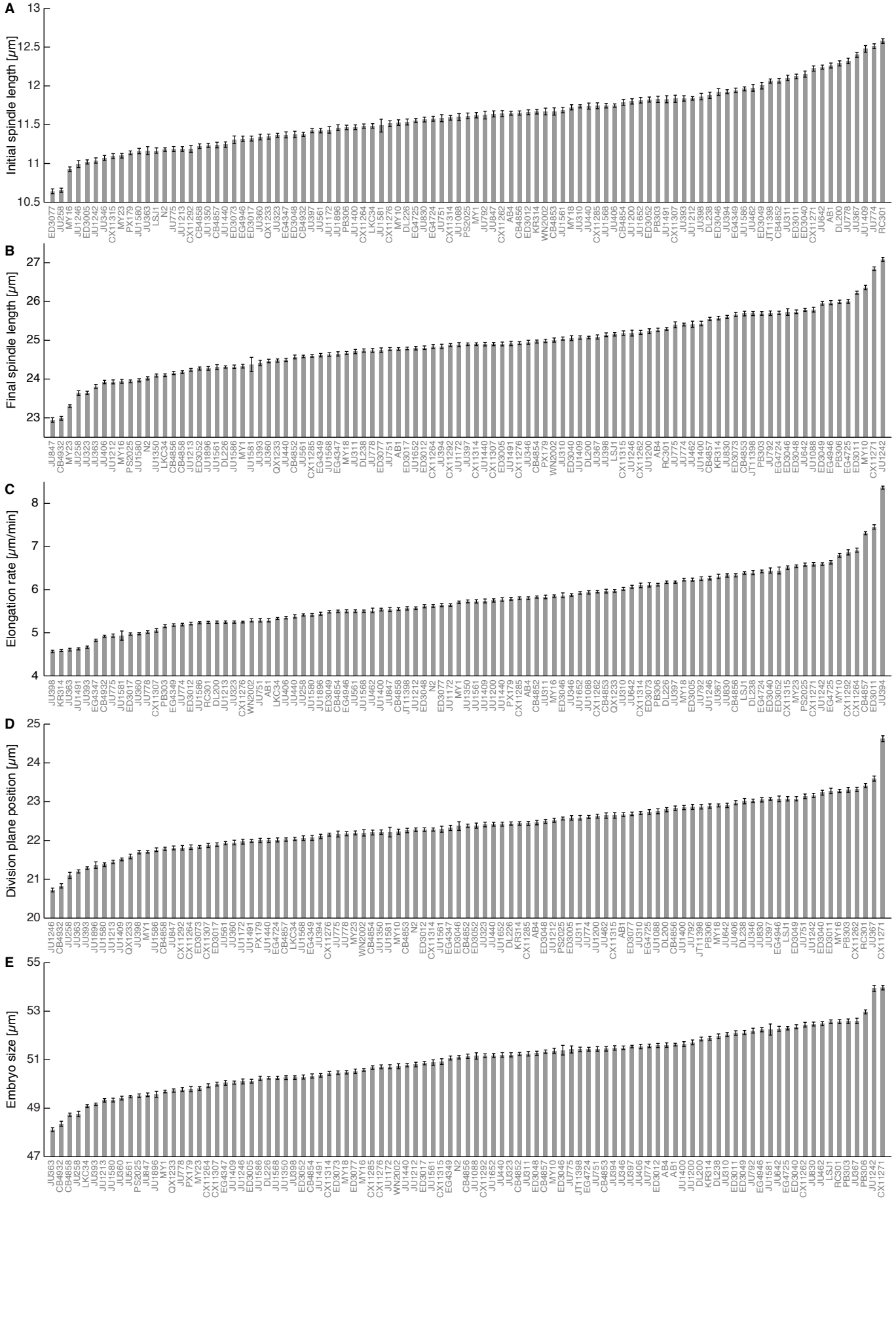
A
Initial spindle length [μm]
13
12.5
12
11.5
11
10.5
ED3077 JU258 MY16 JU1246 ED3005 JU1242 JU346 CX11315 PX123 PS2025 JU1580 JU363 LSJ1 N2 JU775 JU1213 CX11292 CB4858 JU1350 CB4857 JU1440 ED3073 EG4946 ED3017 JU360 QX1233 JU323 EG4347 ED3048 CB4932 JU397 JU561 JU1172 JU1896 PB306 JU1400 CX11264 LKC34 JU1581 CX11276 MY10 DL226 EG4725 JU1652 EG4724 JU751 CX11314 JU1088 PS2025 MY1 JU792 JU847 CX11262 AB4 CB4856 ED3012 KR314 WN2002 CB4853 JU1561 MY18 JU310 JU440 CX11285 JU1568 JU406 CB4854 JU1200 JU1652 ED3052 PB303 JU1491 CX11307 JU393 JU1212 JU398 DL238 ED3046 JU1394 JU1349 JU1588 JU462 ED3049 JT11398 CB4852 JU311 ED3011 ED3040 CX11271 JU642 AB1 DL200 JU778 JU367 JU1409 JU774 RC301
B
Final spindle length [μm]
27
26
25
24
23
JU847 CB4932 MY23 JU258 JU323 JU363 JU406 JU1212 MY18 PS2025 JU1580 N2 JU1350 LKC34 CB4856 CB4858 JU1213 ED3052 JU1896 JU1561 DL226 JU1586 MY1 JU1581 JU393 JU360 QX1233 JU323 JU440 CB4852 JU561 CX11285 EG4349 JU1568 JU1896 EG4347 MY18 JU311 DL238 JU778 ED3077 JU751 AB1 ED3017 JU1652 EG4725 JU1212 EG4724 CX11292 JU1172 JU394 CX11292 JU1172 JU397 CX11314 JU1440 CX11307 ED3005 JU1491 CX11276 JU346 CB4854 PX179 WN2002 JU310 ED3040 JU1561 JU1440 DL200 JU367 JU398 LSJ1 CX11315 JU1246 CX11262 JU1200 AB4 RC301 JU775 JU774 JU462 JU1400 CB4857 KR314 JU1409 JU1349 ED3046 CB4853 JT11398 PB303 JU792 EG4724 ED3046 JU642 JU1088 ED3049 EG4946 PB306 EG4725 ED3011 MY10 CX11271 JU1242
C
Elongation rate [μm/min]
8
7
6
5
4
JU398 KR314 JU363 JU1491 JU393 EG4347 CB4932 JU1212 JU775 JU1561 ED3077 JU360 JU398 CX11307 PB303 EG4349 JU774 ED3012 JU1586 RC301 CX11307 JU561 JU1213 JU323 CX11276 WN2002 JU751 AB1 LKC34 JU406 JU440 JU258 JU1580 JU1896 ED3049 CB4854 EG4946 JU561 JU1568 JU462 JU1400 JU847 CB4858 JT11398 JU1212 ED3048 N2 ED3077 JU1172 MY1 JU1350 JU1561 JU1409 JU1200 JU1440 PX179 CX11285 AB4 CB4852 JU311 MY16 ED3046 JU346 JU1652 JU1088 CX11282 CB4853 QX1233 JU310 JU642 CX11314 ED3073 PB306 DL226 JU387 MY18 ED3005 JU792 JU1246 JU387 KR314 JU1349 CB4856 LSJ1 DL238 EG4724 ED3040 ED3052 CX11315 MY23 PS2025 CX11271 JU1242 EG4725 MY10 CX11292 CX11264 CB4857 ED3011 JU394
D
Division plane position [μm]
25
24
23
22
21
20
JU1246 CB4932 JU258 JU363 JU393 JU1896 JU1580 JU1213 QX1233 JU398 MY1 JU1586 CB4858 JU847 CX11292 CX11264 ED3073 CX11307 ED3017 JU561 JU360 JU1172 JU1491 JT11398 JU1440 EG4724 CB4857 LKC34 JU1652 EG4349 JU394 CX11276 JU775 JU778 MY23 WN2002 CB4854 JU1350 JU1581 MY10 CB4853 N2 ED3012 CX11314 JU1561 EG4347 ED3046 CB4852 ED3052 JU323 JU440 JU1652 DL226 KR314 CX11285 AB4 ED3048 JU1212 PB303 ED3005 JU1568 JU311 JU774 JU1200 JU462 CX11315 AB1 ED3077 JU310 EG4725 JU1088 DL200 CB4856 JU1400 JU792 JT11398 PB306 KR314 JU1349 JU642 JU406 JU1588 DL238 JU346 JU830 JU397 EG4946 LSJ1 ED3049 JU751 JU1242 ED3040 ED3011 MY16 PB303 CX11262 JU1581 RC301 CX11271
E
Embryo size [μm]
55
53
51
49
47
JU363 CB4932 CB4858 JU258 LKC34 JU393 JU1213 JU1580 JU360 JU561 PS2025 JU847 JU1896 MY1 QX1233 JU778 PX179 MY23 CX11264 CX11307 EG4347 JU1409 JU1246 ED3005 JU1586 JU1568 JU1350 JU398 ED3052 CB4854 JU1491 CX11314 ED3073 MY18 ED3077 MY16 CX11285 CX11276 JU1172 WN2002 JU1440 JU1561 ED3012 CX11314 CX11315 EG4349 N2 CB4856 JU1088 CX11292 JU1652 JU440 JU323 CB4852 JU311 ED3048 CB4857 MY10 ED3046 JU775 JT11398 EG4724 JU751 CB4853 JU394 JU346 JU397 JU406 JU774 ED3012 AB4 AB1 JU1400 JU1200 DL200 KR314 DL238 JU830 JU642 ED3011 ED3049 JU792 EG4946 JU1581 JU642 EG4725 ED3040 CX11262 JU830 JU462 LSJ1 RC301 PB303 JU367 JU1242 CX11271

Figure S1: Ranked order variation of cell division traits across *C. elegans* natural isolates, Related to Figure 2. Error bars indicate standard error of the mean.

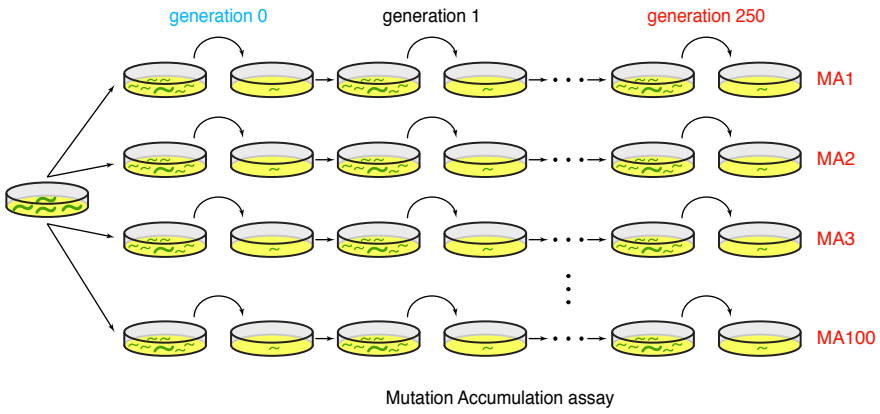

Figure S2: Schematic illustration of mutation accumulation (MA) assay, Related to Figure 3. Starting from a pool of genetically identical worms, MA lines are simultaneously initiated by transferring a randomly selected hermaphrodite in each generation for ~250 generations. Non-lethal and non-sterile spontaneous mutations are allowed to accumulate over time in an effectively neutral fashion. Determining the distribution of a phenotypic trait among the MA lines provides a measure of the effect of spontaneous mutations on that trait.

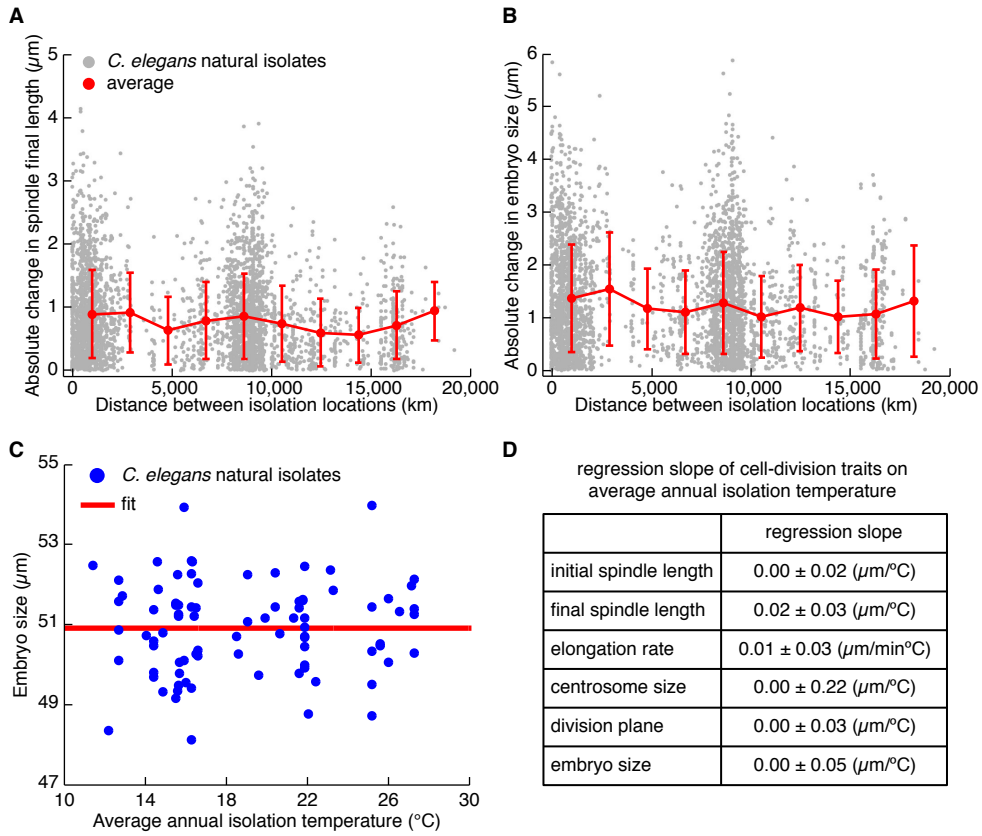

	regression slope
initial spindle length	0.00 ± 0.02 (μm/°C)
final spindle length	0.02 ± 0.03 (μm/°C)
elongation rate	0.01 ± 0.03 (μm/min°C)
centrosome size	0.00 ± 0.22 (μm/°C)
division plane	0.00 ± 0.03 (μm/°C)
embryo size	0.00 ± 0.05 (μm/°C)

Figure S3: Absence of correlation between cell division traits and geographic location and local temperature across *C. elegans* natural isolates, Related to Figure 4. Absolute change in spindle final length (**A**) and embryo size (**B**) as a function of geographic distance of the isolation location between pairs of *C. elegans* natural isolates. No significant correlation was observed for all cell division traits. (**C**) Embryo size as a function of average isolation temperature across *C. elegans* natural isolates. No significant correlation between embryo size and local temperature was observed. (**D**) Table of regression coefficients of cell division traits on average isolation temperature of *C. elegans* natural isolates (mean ± s.e.). No significant correlation between cell division traits and local temperature was observed.

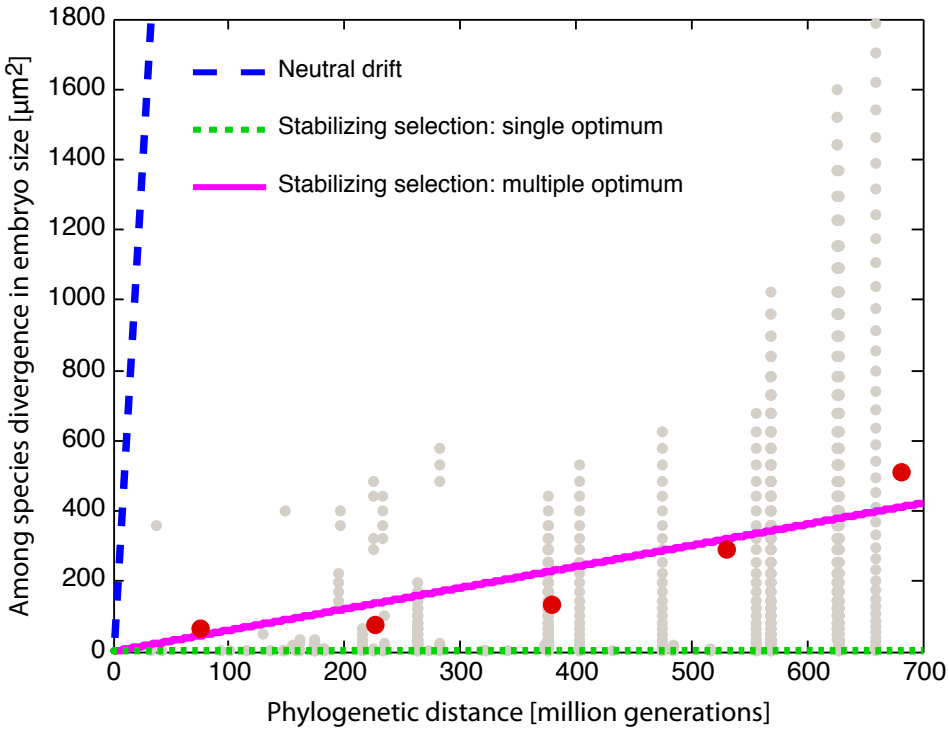

Figure S4: Divergence of embryo size with phylogenetic distance, Related to Figure 5. Divergence of embryo size with phylogenetic distance across different species in Figure 5 is not compatible with expectations of models of neutral drift or stabilizing selection with a single optima, but is consistent with a model of stabilizing selection in which each species has its own optimal embryo size. Gray dots are the divergence in embryo size for pair of species and red dots show the average divergence in embryo size.

	Vp	Vg	Ve	Vm	Δm
Initial Length	0.8 ± 0.03 (μm^2)	0.06 ± 0.01 (μm^2)	0.74 ± 0.03 (μm^2)	7.06E-5 ± 1.07E-4 (μm^2)	-5.91E-5 (μm)
Final Length	1.65 ± 0.07 (μm^2)	0.24 ± 0.04 (μm^2)	1.40 ± 0.05 (μm^2)	4.20E-4 ± 1.72E-4 (μm^2)	1.88E-5 (μm)
Elongation Rate	1.00 ± 0.06 ($\mu m^2/min^2$)	0.20 ± 0.04 ($\mu m^2/min^2$)	0.80 ± 0.04 ($\mu m^2/min^2$)	3.37E-4 ± 7.46E-5 ($\mu m^2/min^2$)	-2.77E-5 (μm/min)
Centrosome Size	37.62 ± 2.89 (μm^4)	6.52 ± 1.37 (μm^4)	31.10 ± 2.03 (μm^4)	4.70E-3 ± 2.50E-3 (μm^4)	1.72E-5 (μm^2)
Division Plane	2.25 ± 0.08 (μm^2)	0.15 ± 0.03 (μm^2)	2.10 ± 0.07 (μm^2)	4.11E-4 ± 1.21E-4 (μm^2)	-3.64E-5 (μm)
Embryo Size	5.72 ± 0.21 (μm^2)	0.55 ± 0.09 (μm^2)	5.17 ± 0.19 (μm^2)	2.17E-3 ± 8.32E-4 (μm^2)	2.60E-5 (μm)

Table S1: Phenotypic variance (Vp), genetic variance (Vg), and environmental variance (Ve) calculated for spindle traits (see Experimental Procedures for details). The amount of genetic variance in a single generation (Vm) and the changes in the traits mean (Δm) generated by spontaneous mutations is shown for each trait (see Experimental Procedures for details). For all traits, the variances are significantly different from zero, while the change in the trait means (Δm) are not significantly different from zero.

S2 A	initial length	final length	elongation rate	centrosome size	division plane	embryo size
initial length	6.14E-2±1.10E-2	3.27E-2±3.05E-2	-1.32E-2±3.04E-2	2.91E-1±1.97E-1	3.04E-2±2.76E-2	6.01E-2±4.53E-2
final length	4.60E-2±4.27E-2	2.44E-1±4.21E-2	6.38E-2±5.81E-2	6.08E-1±3.44E-1	8.78E-2±6.22E-2	2.41E-1±1.15E-1
elongation rate	2.68E-1±7.01E-2	3.11E-1±7.53E-2	1.99E-1±4.15E-2	-4.09E-1±2.12E-1	4.44E-2±5.05E-2	8.07E-2±9.30E-2
centrosome size	2.55E-2±6.92E-2	2.53E-1±8.15E-2	-1.99E-1±5.50E-2	6.52±1.37	9.01E-2±2.54E-1	5.76E-1±4.64E-1
division plane	1.75E-1±4.51E-2	4.04E-1±6.50E-2	2.75E-1±6.91E-2	1.06E-1±6.85E-2	1.51E-1±3.09E-2	2.36E-1±1.01E-1
embryo size	2.22E-1±4.67E-2	7.02E-1±8.18E-2	4.46E-1±7.75E-2	2.40E-1±7.50E-2	7.09E-1±7.36E-2	5.51E-1±9.16E-2

S2 B	initial length	final length	elongation rate	centrosome size	division plane	embryo size
initial length	7.06E-5±1.07E-4	8.44E-5±2.28E-4	-2.00E-5±9.56E-5	2.67E-5±6.19E-4	5.99E-5±1.92E-4	9.28E-5±4.82E-4
final length	5.60E-2±6.48E-2	4.20E-4±1.72E-4	2.38E-4±1.77E-4	8.59E-4±9.18E-4	3.67E-4±2.94E-4	7.75E-4±7.48E-4
elongation rate	2.58E-1±7.81E-2	3.15E-1±9.45E-2	3.37E-4±7.46E-5	1.65E-4±4.58E-4	2.55E-4±1.74E-4	6.92E-4±4.35E-4
centrosome size	5.55E-2±5.90E-2	2.91E-1±8.91E-2	-6.37E-2±6.43E-2	4.70E-3±2.50E-3	1.02E-3±7.63E-4	1.60E-3±1.93E-3
division plane	1.53E-1±6.18E-2	5.00E-1±1.02E-1	2.85E-1±8.11E-2	1.88E-1±7.04E-2	4.11E-4±1.21E-4	9.02E-4±6.60E-4
embryo size	1.83E-1±9.08E-2	7.17E-1±1.48E-1	4.43E-1±1.17E-1	3.11E-1±1.04E-1	7.49E-1±1.43E-1	2.17E-3±8.32E-4

S2 C	initial length	final length	elongation rate	centrosome size	division plane	embryo size
initial length	1.90E-5±4.35E-5	1.04E-4±1.34E-4	-1.88E-5±1.09E-4	-4.84E-5±5.63E-4	3.10E-5±8.99E-5	1.59E-4±2.36E-4
final length	1.86E-2±7.30E-2	1.97E-4±2.14E-4	1.69E-4±2.34E-4	3.70E-5±1.22E-3	2.51E-4±2.44E-4	3.86E-4±6.74E-4
elongation rate	2.73E-1±1.06E-1	2.55E-1±9.87E-2	2.36E-4±1.04E-4	-1.71E-4±5.85E-4	1.39E-4±1.93E-4	4.08E-4±4.61E-4
centrosome size	6.98E-2±8.41E-2	2.84E-1±1.12E-1	-6.95E-2±7.91E-2	5.11E-3±4.07E-3	5.43E-4±9.62E-4	8.27E-4±2.10E-3
division plane	1.56E-1±6.53E-2	4.35E-1±8.97E-2	2.47E-1±8.59E-2	1.50E-1±8.31E-2	3.14E-4±9.92E-5	5.62E-4±4.90E-4
embryo size	1.87E-1±1.01E-1	6.73E-1±1.50E-1	4.23E-1±1.26E-1	2.80E-1±1.15E-1	7.03E-1±1.56E-1	9.87E-4±6.42E-4

S2 D	initial length	final length	elongation rate	centrosome size	division plane	embryo size
initial length	1.22E-4±2.10E-4	6.53E-5±4.36E-4	-2.12E-5±1.57E-4	1.02E-4±1.10E-3	8.87E-5±3.73E-4	2.69E-5±9.34E-4
final length	9.33E-2±1.07E-1	6.44E-4±2.70E-4	3.08E-4±2.65E-4	1.68E-3±1.37E-3	4.83E-4±5.36E-4	1.16E-3±1.34E-3
elongation rate	2.43E-1±1.15E-1	3.76E-1±1.61E-1	4.39E-4±1.07E-4	5.01E-4±7.06E-4	3.72E-4±2.89E-4	9.76E-4±7.37E-4
centrosome size	4.12E-2±8.27E-2	2.99E-1±1.39E-1	-5.80E-2±1.01E-1	4.29E-3±2.89E-3	1.49E-3±1.18E-3	2.37E-3±3.24E-3
division plane	1.49E-1±1.05E-1	5.66E-1±1.82E-1	3.24E-1±1.38E-1	2.25E-1±1.14E-1	5.08E-4±2.22E-4	1.24E-3±1.22E-3
embryo size	1.78E-1±1.51E-1	7.62E-1±2.55E-1	4.64E-1±1.98E-1	3.42E-1±1.73E-1	7.96E-1±2.39E-1	3.34E-3±1.53E-3

Table S2: Matrices of genetic variances (green), covariances (red), and correlation (blue) of cell division traits (A) *C. elegans* natural isolates, (B) average of *C. elegans* N2 and PB306 mutation accumulation lines, (C) *C. elegans* N2 mutation accumulation lines, (D) *C. elegans* PB306 mutation accumulation lines.